AIChE

Link Between Bubbling and Segregation Patterns in Gas-Fluidized Beds with Continuous Size Distributions

Jia Wei Chew and Christine M. Hrenya
Dept. of Chemical and Biological Engineering, University of Colorado at Boulder, Boulder, CO 80309

DOI 10.1002/aic.12507
Published online January 20, 2011 in Wiley Online Library (wileyonlinelibrary.com).

Experiments involving a bubbling, gas-fluidized bed with Gaussian and lognormal particle-size distributions (PSDs) of Geldart Group B particles have been carried out, with a focus on bubble measurements. Previous work in the same systems indicated the degree of axial species segregation varies non-monotonically with respect to the width of lognormal distributions. Given the widely accepted view of bubbles as "mixing agents," the initial expectation was that bubble characteristics would be similarly non-monotonic. Surprisingly, results show that measured bubble parameters (frequency, velocity, and chord length) increase monotonically with increasing width for all PSDs investigated. Closer inspection reveals a bubble-less bottom region for the segregated systems, despite the bed being fully fluidized. More specifically, results indicate that, the larger the bubble-less layer is, the more segregated the system becomes. The direct comparison between bubbling and segregation patterns performed provides a more complete physical picture of the link between the two phenomena. © 2011 American Institute of Chemical Engineers *AIChE J,* 57: 3003–3011, 2011
Keywords: bubbling gas-fluidized bed, axial bubble profile, continuous particle-size distribution (Gaussian, lognormal), Geldart Group B, segregation

Introduction

Gas-solid, dense-phase fluidization finds many applications in industry, including coal combustion and gasification, fluidized catalytic cracking, chemical synthesis, biomass gasification, etc. The reasons for such extensive popularity are the simplicity in geometric configuration, high heat and mass transfer rates, capability of continuous operation, applicability over a wide range of particle properties, to name a few.[1,2] Dense-phase fluidization is a general term which includes particulate fluidization, bubbling fluidization, and turbulent fluidization.[2] The focus of this work is on bubbling, gas-fluidized beds of polydisperse Geldart Group B particles, in which the bubbling behavior and species segregation can significantly affect the performance of the bed in terms of solids mixing, entrainment, and heat and mass transfer.

Species segregation (or demixing) effects are commonplace in systems comprising of various particle sizes. For example, the particles in bubbling fluidized beds are often not monodisperse, which can lead to segregation according to particle size.[3–5] Because bubble characteristics are also known to vary along the height of a bed (e.g., bubbles can grow with height), the gas-solid contact times of segregated particles at the top and the bottom of the bed may vary, thereby impacting the overall efficiency of the unit.

Despite the prevalence of continuous particle-size distributions (PSDs) in industrial fluidized beds, most previous segregation studies have been focused on binary mixtures consisting of two particle types of different sizes and/or densities (for recent review, see Joseph et al.[6]). A natural follow-on

Correspondence concerning this article should be addressed to C. M. Hrenya at hrenya@colorado.edu.

question arises: can previous work on binary mixtures be extrapolated for predicting trends in systems with continuous PSDs? Recent work has shown otherwise.[7] In particular, while binary mixtures have been shown to increasingly segregate with increasing disparity in size and/or density,[3–6] the trend is not so straightforward for continuous distributions. Namely, recent results on continuous PSDs have revealed an unexpected non-monotonic axial segregation behavior with respect to distribution width.[7] This surprising observation provides the motivation for the current effort. In particular, the objective of this work is to better understand the driving force behind the observed non-monotonic segregation behavior, with an eye toward the link between bubbling and species segregation phenomena.

Before discussing the role of bubbles in systems with particles of different sizes and/or material densities, a review of previous findings on bubbles in monodisperse beds is warranted. The bubbles observed in low-velocity, gas-fluidized beds can be traced to an inherent instability of the suspension[8–11] and are believed to be the primary factor associated with solids dispersion, mixing, and reactor efficiency.[1,2,11,12] As early as 1962, Rowe et al.[13] used an X-ray technique to experimentally characterize bubbles in gas-fluidized beds, and the X-ray photographs of bubbles provided evidence that bubbles are primarily responsible for the axial movement of particles in the bed. Since then, detailed experimental observations of the bubbling phenomenon have sprouted,[14–16] including, but not limited to, the volume of the wake behind the bubbles,[17] cloud formation around bubbles,[18,19] bubble coalescence[20–22] and breakage,[23] and exchange between the bubble and emulsion phase.[24–26] Generally, bubbles are commonly referred to as "mixing agents," carrying particles efficiently upwards and allowing particles to fall through them downwards.[13,17,27,28]

For fluidized beds with particles of different sizes, studies on bubbling are scarcer. It has been reported that addition of fines (particle diameter <45 μm) improves mixing,[29–31] and electrical capacitance tomography has further verified that the enhanced mixing is brought about by the increase in the relative proportion of gas flowing interstitially and that the maximum mixing is at a fines content of 15%.[31] More recently, Beetstra et al.[32] determined experimentally the impact of fines and distribution width of Geldart Group A particles on bubbling effects, and it was found that either increasing the width of the PSD or increasing fines amount independently reduced bubble size at high velocity (10 times minimum fluidization velocity, U_{mf}) and enlarged bubble size at low velocity (1.5 U_{mf}). Discrete element models simulations have also indicated that systems with a wider PSD exhibit higher particle velocities around bubbles, resulting in faster bubble growth and its subsequent rise through the fluidized bed.[33] Collectively, these efforts shed light on how the presence of a size distribution alters the bubbling behavior.

Although a direct link between bubbling behavior and species segregation is often presumed, experimental studies with side-by-side measurements of bubble parameters and species segregation are lacking. In an effort to build on previous knowledge on the effect of continuous PSDs on species segregation and bubbling phenomena, the objective of the current work is twofold: (i) to experimentally determine the impact of the width of the PSD on bubble frequency, bubble velocity, and bubble chord length and (ii) to compare the bubble measurements with species segregation measurements. The latter is of particular importance to determine whether bubbles also serve as the primary mixing agents for polydisperse systems. A particularly good test case for this hypothesis is the recent segregation data reported by Chew et al.,[7] which is reproduced in Figure 1. In this figure, the degree of segregation (s_{cont}) vs. distribution width (σ/d_{sm}, where σ is the standard deviation and d_{sm} is the Sauter-mean diameter) is plotted for both Gaussian and lognormal distributions. The quantity s_{cont} is an axial segregation index developed for continuous size distributions,[7] where a value of 0 refers to perfectly-mixed systems and a value of 1 refers to perfectly-segregated systems. The results suggest that, while the level of segregation increases with width for Gaussian distributions, a non-monotonic behavior exists for lognormal distributions. Note that Gaussian distributions with $\sigma/d_{sm} > 30\%$ are not physically possible due to the introduction of negative particle diameters at wider distributions widths. Hence, with regard to objective (ii), the pertinent question is: do bubble parameters (frequency, velocity, and chord length) in systems with Gaussian distributions behave monotonically with respect to distribution width, while the bubbles characteristics behave in a non-monotonic manner with increasing width of lognormal distributions?

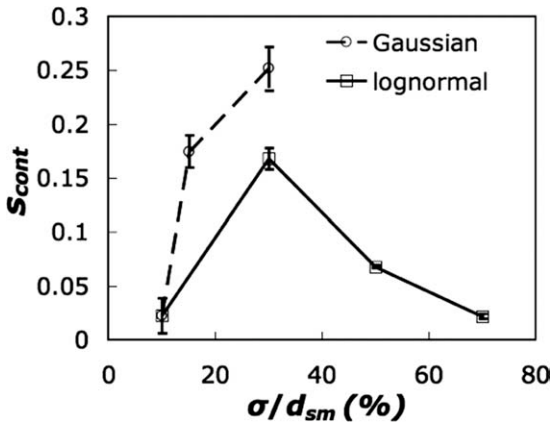

Figure 1. Segregation indices for bubbling, gas-fluidized beds with continuous distributions.[7]

In the current effort, bubbling measurements have been carried out for the same set of systems represented in Figure 1, such that a direct comparison between degree of segregation and bubbling behavior is possible. Surprisingly, the results indicate that bubble parameters (frequency, velocity and chord length) increase monotonically with an increase of PSD widths for all Gaussian and lognormal distributions examined. Accordingly, a direct correlation between measured bubble characteristics and degree of segregation does not exist. More explicitly, even though a non-monotonic correlation between degree of segregation and the width of lognormal distribution was observed, the bubbling parameters show a monotonic increase with PSD width. Nonetheless, a more careful examination of the data reveals the presence of a bubble-less layer in segregated systems. The height of this bubble-less layer is tightly coupled to the degree of segregation, thereby providing the sought-after physical link between bubbling and segregation patterns.

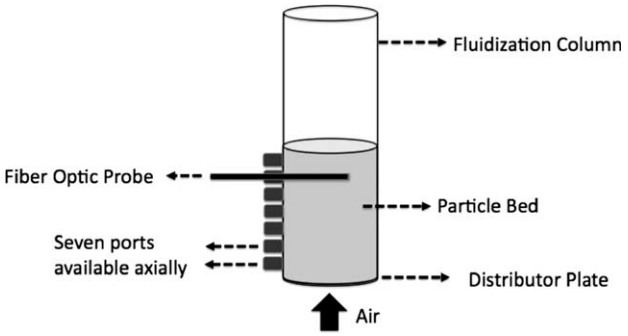

Figure 2. Experimental set-up.

Experimental Description

Fluidized bed setup

The experimental setup for all bubbling experiments is identical to that used by Chew et al.[7] for the corresponding segregation experiments. Namely, as illustrated in Figure 2, the fluidization column is made of Plexiglass with an inner diameter of 18.5 cm, and a sintered metal plate (20 nominal microns) at the bottom that serves as a distributor plate. The uniform distribution of air by the distributor plate was ascertained by ensuring that the pressure drop across the plate was at least 100% that across the bubbling bed. Seven ports, spaced 2.54 cm axially apart and the lowest of which is 5.08 cm above the distributor plate, are available for insertion of the fiber optic probe, which is used for detecting bubbles.

Continuous size distributions of sand were first prepared with various distribution widths, defined as the ratio of standard deviation to Sauter-mean diameter (σ/d_{sm}). Figure 3 shows the continuous distributions investigated. Notably, the Sauter-mean diameter (d_{sm}) of all the Gaussian and lognormal distributions under investigation was set to 375 μm,[7] which is the middle value of the Geldart Group B size range. To ensure a wide range of distributions widths, Gaussian distributions with σ/d_{sm} ranging from 10 to 30% and lognormal distributions with σ/d_{sm} ranging from 10 to 70% were investigated.[7] Notably, Gaussian distributions with $\sigma/d_{sm} > 30\%$ are not physically possible due to the necessity of introducing negative particle diameters. In addition, although all the Gaussian distributions are classified as Geldart Group B particles, the wider lognormal distributions ($\sigma/d_{sm} \geq 50\%$) contain up to 20% by mass of Geldart Group D particles, since the entire Geldart Group B range was not wide enough to contain the full distribution of particle sizes.

For the previous segregation experiments[7] (the data from which will be compared to the bubbling measurements described herein), axial segregation profiles were obtained via the ''frozen–bed'' sectioning method. Namely, the bubbling bed was operated for a period long enough to ensure that a statistical steady-state was reached, after which the gas velocity was abruptly turned off. Axial sections of the frozen (settled) bed were analyzed for particle-size distribution using sieving. It is important to mention that because the superficial gas velocities were restricted to small values, segregation upon free-fall was effectively eliminated. Further details on the experimental protocol can be found in Chew et al.[7]

In this work, the objective is to obtain bubble measurements for the same systems described above. Accordingly, the experimental protocol is similar to that in Chew et al.,[7] except that a fiber optic probe is utilized to obtain information on the bubble characteristics. Namely, for each experiment, 8 kg of sand was used. At the start of each run, the fiber optic probe was inserted into one of the seven ports, and positioned such that the probe tip was flush with the inner wall of the column. Then, the prepared distribution of sand was placed in the column. Next, the particle bed was mixed at high velocity [three times superficial velocity for complete fluidization ($3U_{cf}$)] for 15 minutes, and then fluidized at 1.2 U_{cf} for 1 hour to achieve a statistical steady-state. More specifically, U_{cf} is defined as the velocity beyond which pressure drop across the bed (ΔP_{bed}) equals to the ratio of the bed weight to cross-sectional area of the column (W/A). For the distributions investigated, the U_{cf} values are similar at ~0.12 m/s; U_{cf} are expectedly similar, because the distributions are centered about the same mean particle size (d_{sm}).[34,35] Afterwards, the fiber optic probe was positioned sequentially at each of the nine radial positions to collect

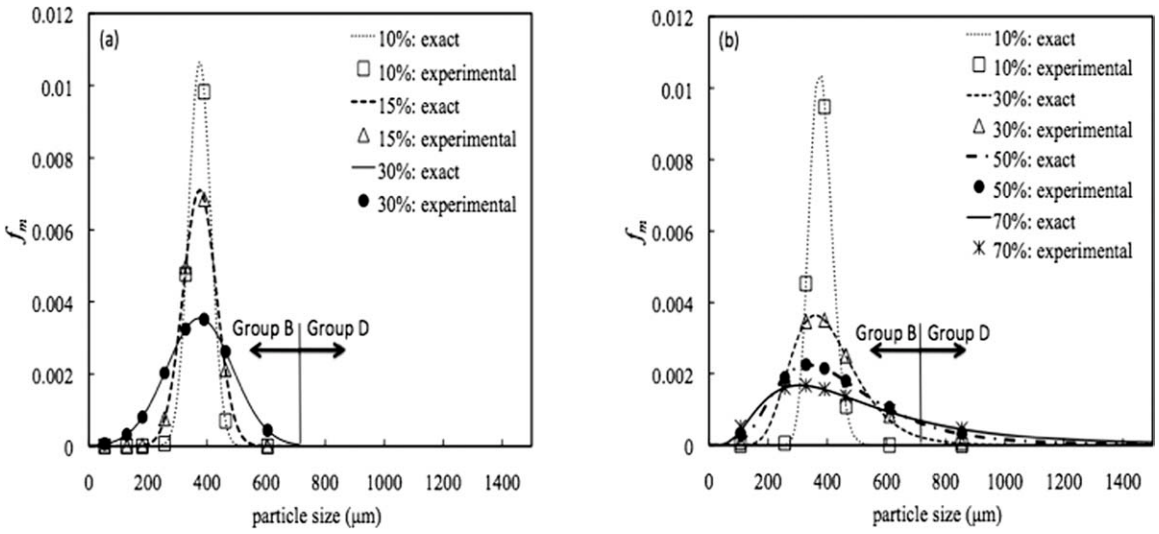

Figure 3. Gaussian and lognormal distributions investigated.

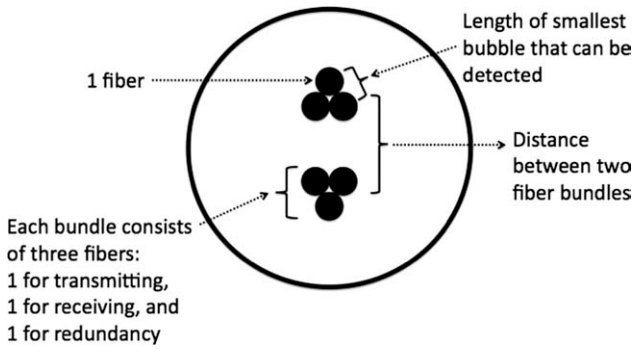

Figure 4. Schematic of tip of fiber optic probe.

data for 1 minute. The same protocol was then repeated for the other axial locations. To obtain reasonable 95% confidence intervals of the data, each measurement was repeated 10 times.

Fiber optic probe and signal analysis

With regards to the fiber optic probe, it consists of two bundles of fibers, one positioned vertically above the other. Each bundle contains three fibers: one fiber is used to transmit the light source, the second is the receiver conduit, while the third is redundant but is an important spare, as displayed in Figure 4. A higher voltage signal is obtained from the receiving fiber when light emitted from the light-source fiber is blocked, as occurs when the probe is surrounded by the emulsion (particle-rich) phase. On the other hand, a lower voltage signal is obtained when light from the emitter is relatively unobstructed, which occurs when the probe tip is surrounded by a bubble. Hence, as illustrated in the voltage traces of the bottom and top fiber bundles given in Figure 5, which is a plot of voltage measured by the probe vs. time, bubbles appear as downward spikes in the voltage signal. Information about the bubbles can thus be extracted by defining a threshold voltage value ($V_{\text{threshold}}$), which serves as a demarcation between bubbles and the emulsion phase.

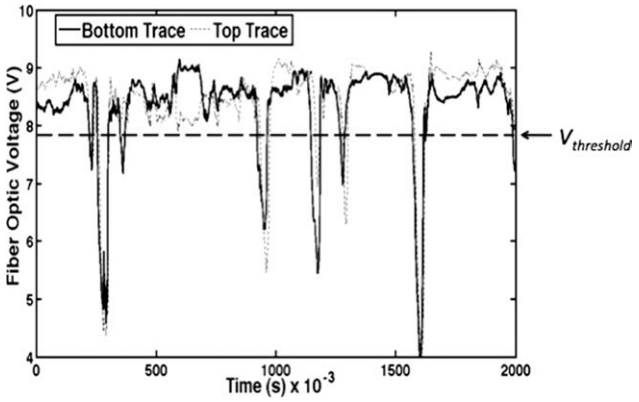

Figure 5. Example of bubble trace obtained from fiber optic probe: voltage vs. time for top and bottom bundle, where $V_{\text{threshold}}$ indicates the demarcation between bubble (below) and emulsion (above) phase.

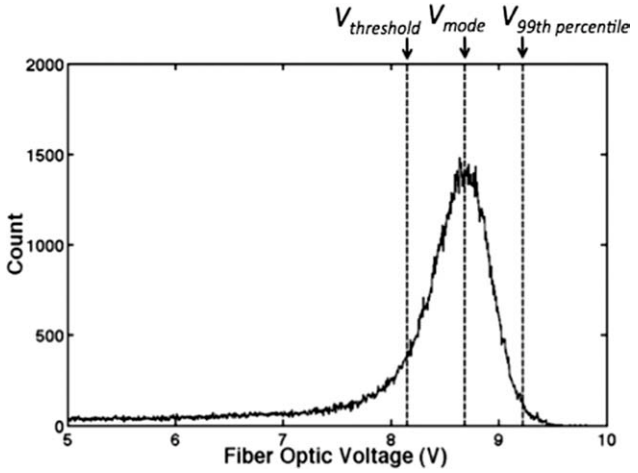

Figure 6. Probability distribution function (PDF) of bubble trace, with $V_{\text{threshold}}$, V_{mode}, and $V_{\text{99th-percentile}}$ marked.

As demonstrated in Figure 6, $V_{\text{threshold}}$ is determined by first plotting the probability density function (PDF) of the voltage trace obtained from the fiber optic probe at increments of 0.001s. Then, the mode of the PDF and the 99th percentile of the cumulative count are determined. Finally, $V_{\text{threshold}}$ is calculated as the voltage at which the voltage difference (ΔV) between V_{mode} and $V_{\text{99th-percentile}}$ is the same as that between V_{mode} and $V_{\text{threshold}}$, namely

$$\Delta V = V_{\text{99th percentile}} - V_{\text{mode}} \tag{1}$$

$$V_{\text{threshold}} = V_{\text{mode}} - \Delta V \tag{2}$$

With this value of $V_{\text{threshold}}$ at hand, a ''bubble-only'' trace can be obtained by eliminating the portions of the trace above $V_{\text{threshold}}$. From the bubble-only traces of the top and bottom fiber bundles, the frequency of bubbling, duration of each bubble, and bubble velocity can be found, as described below. In particular, analysis of these traces do not give bubble size per se, but instead bubble chord length, which is an indicator of bubble size.[36,37]

With regards to bubble frequency, the number of segments of continuous data points above $V_{\text{threshold}}$ is counted, then normalized by measurement duration. As for vertical velocity of the bubble, when both the distance between the fiber bundles (Figure 4) and the time lapse between the voltage signals obtained by the bottom and top bundles are known, velocity can be derived. The distance between fiber bundles is measured to be 0.25 cm, while the time lapse is derived by cross-correlating the two signals to find where the point of strongest correlation lies. The cross-correlation formula is given as

$$\chi = \frac{\frac{1}{n}\sum_{i=1}^{n-d}(x_i - x_{\text{mean}})(y_{i+d} - y_{\text{mean}})}{\sigma_x \sigma_y} \tag{3}$$

where χ is the cross-correlation function, n is the total number of data points in each signal, d is the time lapse in units of data points being compared between the two signals, x_i and y_{i+d} are

the bottom and top signal voltages respectively at time i and $i+d$, x_{mean}, and y_{mean} are the mean of the bottom and top signal voltages respectively, and σ_x and σ_y are the standard deviation of each signal trace. $\chi = 1$ implies perfect correlation between the bottom and top signals, i.e. no time lapse. Dividing the distance between the fiber bundles (namely, 0.25 cm) by the time lapse derived by Equation (3) hence gives the vertical velocity of the bubbles. Then, bubble chord lengths can be obtained by multiplying the vertical velocity by durations of each segment of continuous data points above $V_{threshold}$.

Validation of fiber optic data for all bubble parameters considered here (frequency, velocity and chord lengths of bubbles) was obtained via comparison with existing correlations for monodisperse Group B particles (for example, see results of Hiraki and Kunii,[38] Hilligardt and Werther,[39] Mori and Wen,[40] as presented in Kunii and Levenspiel,[1] for bubble frequency, velocity, chord length respectively). It is also worth noting that previous work[36] has shown that chord length can be used as a reliable indicator of bubble size for a given particle shape even if the bubble also has a horizontal component of velocity; for purposes of this work, however, only the direct measurement of chord length will be reported.

Results and Discussion

Experiments to obtain bubble data were carried out in an attempt to better understand the previously-reported, counter-intuitive segregation behavior displayed in Figure 1, namely the non-monotonic segregation levels observed with increases in the width of lognormal distributions. Accordingly, the experimental conditions were identical to those described by Chew et al.[7] The initial hypothesis being tested stems from the physical picture of bubbles as mixing agents. In other words, would the previously observed segregation patterns correlate with bubbling characteristics—e.g., are higher bubbling frequencies observed in the more well-mixed systems? For this hypothesis to hold, bubbling parameters (some or all) should vary monotonically with PSD widths for Gaussian distributions and non-monotonically for lognormal distributions, analogous to the previously reported segregation trends (Figure 1). With this in mind, the bubbling characteristics (bubble frequency, velocity, and chord length) are presented as follows for both Gaussian and lognormal distributions of varying widths.

Before considering each bubble characteristic in turn, it is worthwhile to compare the axial and radial variations of the bubble quantities being measured. For purposes of illustration, a plot of mean bubble chord length vs. dimensionless radius (r/R) is depicted in Figure 7, with error bars representing 95% confidence intervals. It is observed that mean bubble chord length increases with bed height, which is not surprising because bubbles are known to grow axially throughout a bed consisting of Geldart Group B particles.[1,2] Radial variation in bubble chord lengths is minimal compared to the noted axial variation, which is consistent with previous segregation results in which radial segregation was found to be negligible vis-à-vis axial segregation.[7] This consistency between bubbling and segregation results is not surprising since bubbles are often viewed as mixing agents. Consequently, since radial variation of bubbling characteristics (namely, frequency, velocity, and chord length) is negligible, the focus of the following discussion will be on axial variation.

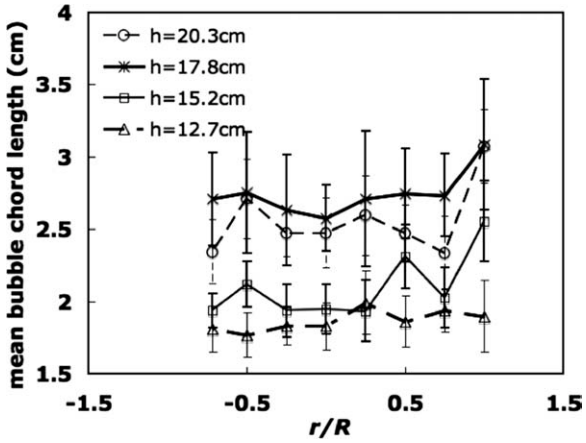

Figure 7. Radial profiles of mean bubble size profiles at each axial position for Gaussian distribution with σ/d_{sm} = 30%.

The bubble characteristics measured for Gaussian distributions with σ/d_{sm} = 10–30% are shown in Figures 8–10, which are plots of bed height (h) vs. bubble frequency, bubble velocity and bubble chord length, respectively. Error bars represent 95% confidence intervals. Analogously, Figures 11–13 contain similar plots for lognormal distributions with σ/d_{sm} in the range of 10–70%. It should be noted that the larger error bars for the widest lognormal distribution of σ/d_{sm} = 70% should be expected, since biggest bubble chord lengths are found in this distribution, which implies a greater variation of chord lengths measured. Collectively, it is observed in Figures 8–13 that bubble frequency, velocity and chord length increase monotonically with increase in PSD width for both Gaussian and lognormal PSDs. Because the previously reported degree of segregation for lognormal distributions is non-monotonic with respect to PSD width, the original anticipation that (some or all) bubble characteristics would be similarly be non-monotonic does not hold.

Since bubbles have been known to play an important role in segregation behavior, it is worthwhile to take a more detailed look at the bubble trends to see if they are consistent with expectations. In particular, for both Gaussian PSDs and the narrower ($\sigma/d_{sm} \leq 30\%$) lognormal PSDs, the bubble characteristics vary monotonically with distribution width, as did the previously reported segregation measurements.[7] So the question remains: does the direction (increasing or decreasing) of the bubble trends make sense in light of the segregation data? More specifically, since bubbles are known to be "mixing agents," an increase in the frequency and velocity of bubbles is presumed to enhance mixing, and vice versa.

Because an increase in the width of a Gaussian PSD was found to lead to increased segregation (Figure 1), it was initially expected that bubble frequency and velocity would decrease with increasing PSD width. Surprisingly, it is observed in Figures 8 and 9 that as the width of the Gaussian PSD increases, the frequency and velocity of the bubbles increase too. With regards to bubble sizes, bigger bubble sizes are expected to enhance mixing: Rowe et al.[28] asserted that the most important mechanism for transporting particles up the bed is by the bubble wake, which is ~20% of the volume

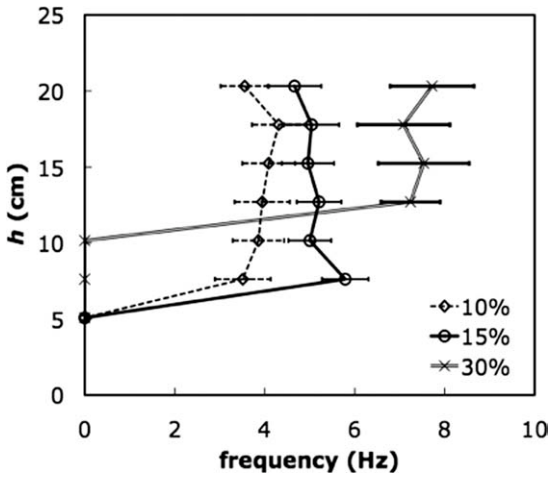

Figure 8. Axial profiles of bubble frequency for Gaussian distributions.

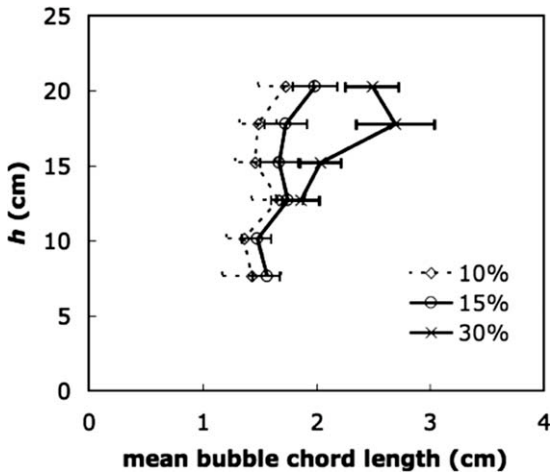

Figure 10. Axial profiles of bubble size for Gaussian distributions.

of bubbles for the size range investigated here.[17] Nevertheless, Figure 10 illustrates that bubble chord length increases with PSD width (consistent with previously reported work on Group A particles[32]), which thus does not seem to explain the increasing segregation extent. Hence, the results indicate that, not only is there a lack of correlation between bubbling and segregation phenomena, but even for the distributions (Gaussian) where there is a correlation, the trends are opposite of expectation. A similarly puzzling observation is observed for lognormal distributions over the range in distribution widths associated with increasing extent of segregation (σ/d_{sm} = 10–50%). Namely, the bubble frequency, velocity, and chord length increase with distribution width (Figures 11–13, respectively), which is seemingly contrary to the increasing levels of segregation (Figure 1). In particular, for the range of lognormal distributions investigated, bubbling is largely monotonic with an increase in width but segregation is not.

A more careful look at the bubble measurements holds the key to understanding the link between bubbling and segregation patterns. Bubbles indeed serve as mixing agents, but the observed segregation is due instead to the absence of bubbles. In particular, a bubble-less layer—a bottom region of the bubbling bed where bubbles are not detected by the fiber optic probe—is observed in some systems. Specifically, the bubble-less region is where zero bubble frequency is detected, as evidenced in Figures 8 and 11; the corresponding velocity and chord length are not plotted, as these parameters are not relevant in the absence of bubbles. This layer is evidenced in Figures 8–10 for Gaussian systems. The largest bubble-less layer is observed for σ/d_{sm} = 30%, in which bubbles are not detected for the three lowest axial positions, whereas only the lowest axial position appears bubble-less for σ/d_{sm} = 10 and 15%. This trend in the bubble-less layers corresponds directly to segregation levels, which is greatest for σ/d_{sm} = 30% in the Gaussian system. A similar correspondence is noted for the lognormal systems across all distribution widths. Recall from Figure 1 that the segregation behavior is surprisingly non-monotonic with respect to PSD width for the lognormal distributions, with segregation extent peaking for the lognormal distribution with σ/d_{sm} = 30%. Figures 11–13 illustrate that the most

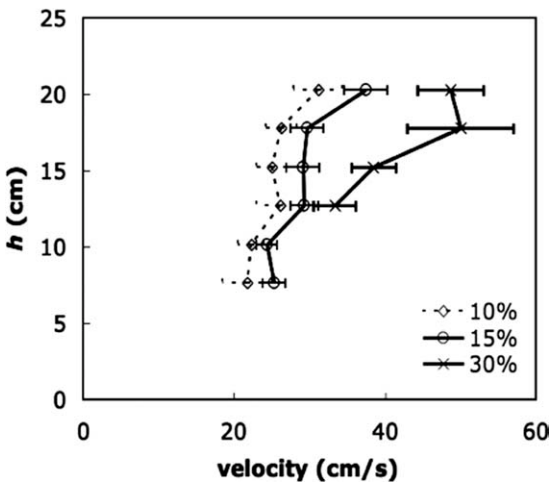

Figure 9. Axial profiles of bubble velocity for Gaussian distributions.

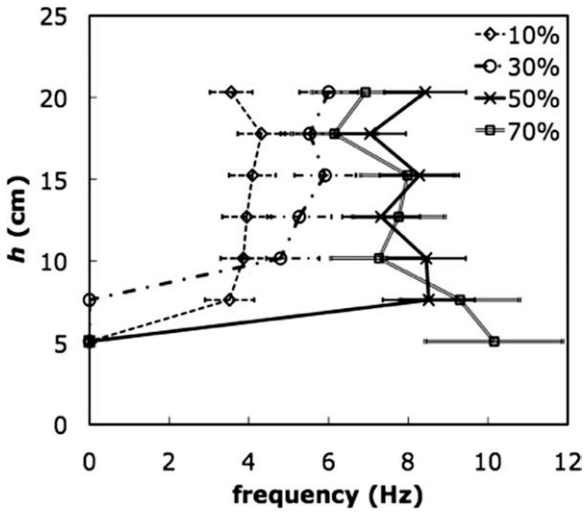

Figure 11. Axial profiles of bubble frequency for lognormal distributions.

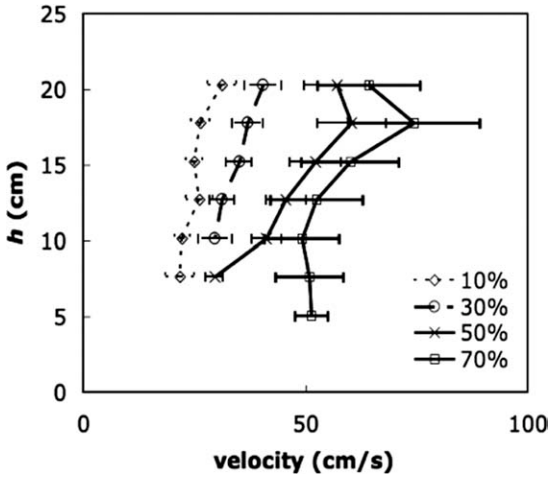

Figure 12. Axial profiles of bubble velocity for lognormal distributions.

segregated lognormal distribution of $\sigma/d_{sm} = 30\%$ has the largest bubble-less layer. While bubbles are detected from the second lowermost position upwards for the more uniformly mixed lognormal distributions of $\sigma/d_{sm} = 10$, 50, and 70%, bubbles can only be detected from the third lowermost position upwards for the lognormal distribution of $\sigma/d_{sm} = 30\%$. Hence, the experimental data conclusively show that regardless of the magnitude of the bubble parameters measured in the upper layer, the larger the bubble-less layer, the more segregated a system becomes.

Two additional points are worth commenting regarding this link between the size of the bubble-less layer and the extent of segregation. First, although bubbles are not detected in the bottom layer, it is important to note that the entire bed (including the bottom layer) is known to be completely fluidized, because the pressure drop across the bed (ΔP_{bed}) is equal to the ratio of the bed weight to the cross-sectional area of the column (W/A) at the operating superficial gas velocity (U_s). Second, the failure to detect bubbles can be traced to either bubbles being nonexistent or bubbles being smaller than

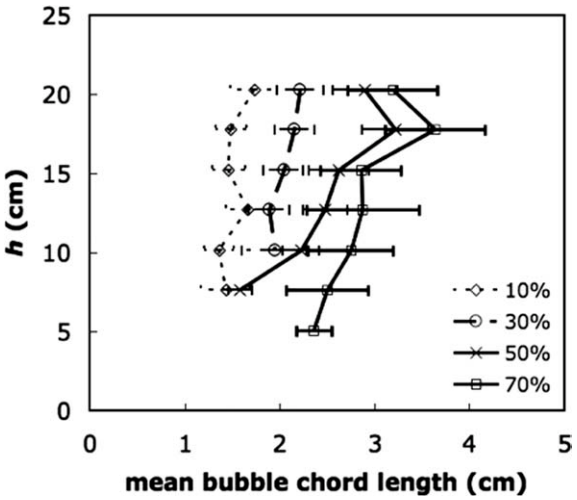

Figure 13. Axial profiles of bubble size for lognormal distributions.

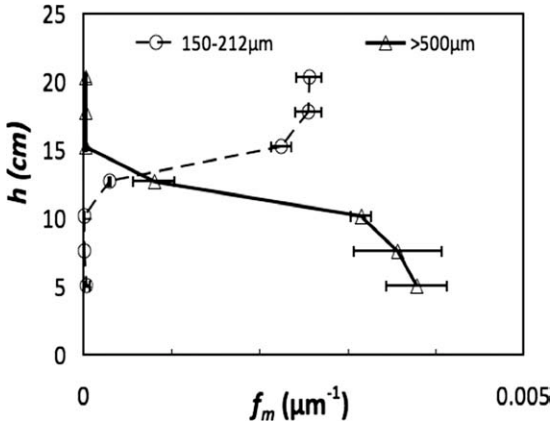

Figure 14. Axial segregation profile of the finest and coarsest species for Gaussian distribution with $\sigma/d_{sm} = 30\%$.

0.1 cm, which is the separation between two fibers in each bundle (Figure 4). Regardless of the situation, however, mixing by bubbles will be ineffective in the bottom layer. More specifically, consider liquid–solid fluidized beds which do not exhibit the bubbling behavior. Such systems are known to display species segregation, which can be traced to the drag force descriptions for each species. This driving force for species segregation will also be present in gas-fluidized beds regardless of whether or not bubbles are present. When bubbles are present, however, their motion induces mixing of the various species. Accordingly, in the bottom bubble-less layer, the segregation mechanism dominates, resulting in a gradient of concentration across that layer (Figure 14). Along the same lines, in the upper bubbling layer, the mixing mechanism dominates, resulting in a well-mixed layer (note vertical nature of concentration profiles in upper layer of Figure 14).

Given that the presence of bubble-less bottom regions provides a link between the observed bubbling behavior and (integrated) segregation index, it is useful to see how the axial profiles of each compare. Figure 14 is a plot of the axial segregation profiles of two different size species for the Gaussian distribution with $\sigma/d_{sm} = 30\%$. The y-axis is the height of the particle bed (h), and the x-axis represents mass-based frequency (f_m), which is the mass fraction of the species normalized with respect to bin sizes. As depicted in Figure 14, two distinct layers of almost constant species concentration is observed, which has been similarly reported before for continuous PSDs.[7,41] Interestingly, but perhaps unsurprisingly, the range of heights over which the transition between the two distinct regions in Figure 14 arises ($h \sim$ 10–15 cm) corresponds exactly to the h range at which transition from bubble-less to bubbling regimes for the same Gaussian distribution with $\sigma/d_{sm} = 30\%$ (Figures 8–10). Other Gaussian and lognormal distributions similarly illustrate that the transition height between bubble-less and bubbling regime corresponds to the transition height between the two distinct layers in the axial segregation profiles.[7]

Concluding remarks

Although bubbles are widely viewed as mixing agents, a direct comparison between the species segregation trends in

systems with continuous PSDs and corresponding bubble characteristics has been lacking. The previously-reported, non-monotonic segregation behavior[7] (with respect to distribution width) for lognormal distributions provides a unique case study for testing the presumed link between segregation and bubble patterns. Hence, experiments involving low-velocity, bubbling, gas-fluidized beds have been carried out for Geldart Group B particles of various widths of Gaussian and lognormal distributions, with a focus of comparing axial segregation to bubble profiles.

Measured bubble parameters (frequency, velocity, and chord length) for the Gaussian (σ/d_{sm} = 10, 15, and 30%) and lognormal (σ/d_{sm} = 10, 30, 50, and 70%) distributions are reported. A somewhat surprising initial observation is the lack of correlation between the degree of segregation and the measured bubble parameters, with respect to distribution width. In particular, although the lognormal distribution displays a non-monotonic degree of segregation as the distribution width is increased, all measured bubble parameters are found to increase over the entire range of distribution widths explored. Nonetheless, the key to understanding the segregation patterns is tied to the presence of a bubble-less layer at the bottom of the (fully-fluidized) bed. Namely, the degree of segregation is strongly tied to the height of the bubble-less layer at the bottom of the bed. For well-mixed systems (i.e., Gaussian distribution with σ/d_{sm} = 10%, and lognormal distributions with σ/d_{sm} = 10% and σ/d_{sm} = 70%), bubbles are present axially throughout most of the bed, hence enabling thorough mixing. For the most segregated systems among the Gaussian and lognormal distributions (σ/d_{sm} = 30%), the largest bubble-less bottom layer is observed, where although the entire bed is fully fluidized, bubbles are either absent or so small (<0.1 cm) that they cannot be detected. Hence, the larger the bubble-less layer at the bottom of the bed, the more segregated the system becomes. Another new finding resulting from this work is the monotonic increase in all bubble parameters (frequency, velocity, and chord length) with respect to PSD width.

Finally, the results of this work are expected to contribute towards the validation of discrete element models and two-fluid models for continuous PSDs. To date, the vast majority of modeling efforts have focused on binary mixtures, and various closures (kinetic theory for collisional stresses, frictional stress, drag laws, etc.) required for adaptation to continuous PSDs remain largely untested, partly due to the lack of detailed experimental data-like that reported in this work. Model validation can proceed on multiple fronts using this dataset: existence of a bubble-less layer, trends of bubble characteristics with widths of distributions, link between segregation and bubbling profiles, etc.

Acknowledgments

The authors gratefully acknowledge the funding from the Department of Energy (DE-FC26-07NT43098) and National Science Foundation (CBET0658903).

Literature Cited

1. Kunii D, Levenspiel O. *Fluidization Engineering*. 2nd ed. Boston: Butterworth-Heinemann, 1991.
2. Fan LS, Zhu C. *Principles of Gas-Solid Flows*, *Chapter 9*. Cambridge UK, Cambridge University Press, 1998.
3. Rowe PN, Nienow AW. Particle mixing and segregation in gas-fluidized beds—review. *Powder Technol*. 1976;15:141–147.
4. Tang P, Puri VM. Methods for minimizing segregation: a review. *Particulate Sci Technol*. 2004;22:321–337.
5. Cui HP, Grace JR. Fluidization of biomass particles: a review of experimental multiphase flow aspects. *Chem Eng Sci*. 2007;62:45–55.
6. Joseph GG, Leboreiro J, Hrenya CM, Stevens AR. Experimental segregation profiles in bubbling gas-fluidized beds. *AIChE J*. 2007; 53:2804–2813.
7. Chew JW, Wolz J, Hrenya CM. Axial segregation in bubbling gas-fluidized beds with Gaussian and lognormal distributions of Geldart Group B particles. *AIChE J*. 2010;3049–3061.
8. Davidson JF, Harrison D, Carvalho JRFGD. Liquid-like behavior of fluidized-beds. *Annu Rev Fluid Mech*. 1977;9:55–86.
9. Jackson R. *The Dynamics of Fluidized Particles*, *Chapter 5*. Cambridge UK, Cambridge University Press, 2000.
10. Sundaresan S. Instabilities in fluidized beds. *Annu Rev Fluid Mech*. 2003;35:63–88.
11. Yang W. *Handbook of Fluidization and Fluid-Particle Systems*, *Chapters 1–2*. New York: Marcel Dekker, 2003.
12. Kunii D, Levenspiel O. *Fluidization Engineering*, 2nd ed. Boston: Butterworth-Heinemann, 1991.
13. Rowe PN, Partridge BA, Ardran GM, Lyall E. Bubbles in fluidized beds. *Nature*. 1962;195:278–279.
14. Cheremisinoff NP. Review of experimental methods for studying the hydrodynamics of gas solid fluidized-beds. *Ind Eng Chem Process Des Dev*. 1986;25:329–351.
15. van Ommen JR, Mudde RF. Measuring the gas-solids distribution in fluidized beds-a review. *Int J Chem React Eng*. 2008;6:Review R3.
16. Mudde RF. Time-resolved X-ray tomography of a fluidized bed. *Powder Technol*. 2010;199:55–59.
17. Rowe PN, Partridge BA. An X-ray study of bubbles in fluidised beds. *Trans Inst Chem Eng Chem Eng*. 1965;43:T157–T175.
18. Rowe PN, Partridge BA, Lyall E. Cloud formation around bubbles in gas fluidized beds. *Chem Eng Sci*. 1964;19:973–985.
19. Partridge BA, Rowe PN. Analysis of gas flow in a bubbling fluidised bed when cloud formation occurs. *Trans Inst Chem Eng Chem Eng*. 1966;44:T349–T358.
20. Clift R, Grace JR. Bubble coalescence in fluidized beds—comparison of 2 theories. *AIChE J*. 1971;17:252–254.
21. Halow JS, Nicoletti P. Observations of fluidized-bed coalescence using capacitance imaging. *Powder Technol*. 1992;69:255–277.
22. Muller CR, Davidson JF, Dennis JS, et al. Real-time measurement of bubbling phenomena in a three-dimensional gas-fluidized bed using ultrafast magnetic resonance imaging. *Phys Rev Lett*. 2006;96: 154504.
23. Clift R, Grace JR. Mechanism of bubble break-up in fluidized-beds. *Chem Eng Sci*. 1972;27:2309–2310.
24. Chiba T, Kobayash H. Gas exchange between bubble and emulsion phases in gas-solid fluidized beds. *Chem Eng Sci*. 1970;25: 1375–1385.
25. Gibilaro LG, Rowe PN. Model for a segregating gas fluidized-bed. *Chem Eng Sci*. 1974;29:1403–1412.
26. Basesme EA, Levy EK. Solids exchange between the bubble wake and the emulsion phase in a 2-dimensional gas-fluidized bed. *Powder Technol*. 1992;72:45–50.
27. Rowe PN, Partridg. Ba, Cheney AG, Henwood GA, Lyall E. Mechanisms of solids mixing in fluidised beds. *Trans Inst Chem Eng Chem Eng*. 1965;43:T271–T286.
28. Rowe PN, Agbim AJ, Nienow AW. Mechanisms by which particles segregate in gas fluidized-beds—binary-systems of near-spherical particles. *Trans Inst Chem Eng Chem Eng*. 1972;50:310–323.
29. Rowe PN, Santoro L, Yates JG. Division of gas between bubble and interstitial phases in fluidized-beds of fine powders. *Chem Eng Sci*. 1978;33:133–140.
30. Yates JG, Newton D. Fine particle effects in a fluidized-bed reactor. *Chem Eng Sci*. 1986;41:801–806.
31. Du B, Fan LS, Wei F, Warsito W. Gas and solids mixing in a turbulent fluidized bed. *AIChE J*. 2002;48:1896–1909.
32. Beetstra R, Nijenhuis J, Ellis N, van Ommen JR. The influence of the particle size distribution on fluidized bed hydrodynamics using high-throughput experimentation. *AIChE J*. 2009;55:2013–2023.
33. Tagami N, Mujumdar A, Horio M. DEM simulation of polydisperse systems of particles in a fluidized bed. *Particuology*. 2009;7:9–18.

34. Sun GG, Grace JR. The effect of particle-size distribution on the performance of a catalytic fluidized-bed reactor. *Chem Eng Sci*. 1990;45:2187–2194.
35. Gauthier D, Zerguerras S, Flamant G. Influence of the particle size distribution of powders on the velocities of minimum and complete fluidization. *Chem Eng J*. 1999;74:181–196.
36. Clark NN, Turton R. Chord length distributions related to bubble-size distributions in multiphase flows. *Int J Multiphase Flow*. 1988;14:413–424.
37. Liu WD, Clark NN, Karamavruc AI. Relationship between bubble size distributions and chord-length distribution in heterogeneously bubbling systems. *Chem Eng Sci*. 1998;53:1267–1276.
38. Hiraki I, Kunii D. Behavior of bubbles in fluidized beds. *Chem Eng Tokyo*. 1969;33:681.
39. Hilligardt K, Werther J. Local bubble gas hold-up and expansion of gas/solid fluidized beds. *German Chem Eng*. 1986;9:215–221.
40. Mori S, Wen CY. Estimation of bubble diameter in gaseous fluidized-beds. *AIChE J*. 1975;21:109–115.
41. Hoffmann AC, Romp EJ. Segregation in a fluidized powder of a continuous size distribution. *Powder Technol*. 1991;66:119–126.

Manuscript received May 29, 2010, revision received Oct. 22, 2010, and final revision received Dec. 6, 2010.